View metadata, citation and similar papers at core.ac.uk
brought to you by CORE
provided by Elsevier - Publisher Connector

Chinese Journal of Aeronautics, (2015), 28(6): 1766–1773

Chinese Society of Aeronautics and Astronautics
& Beihang University

Chinese Journal of Aeronautics

cja@buaa.edu.cn
www.sciencedirect.com

Chatter stability prediction in four-axis milling of aero-engine casings with bull-nose end mill

Zhou Xu, Zhang Dinghua *, Luo Ming, Wu Baohai

Key Laboratory of Contemporary Design and Integrated Manufacturing Technology, Ministry of Education, Northwestern Polytechnical University, Xi'an 710072, China

Received 26 January 2015; revised 4 March 2015; accepted 13 March 2015
Available online 20 June 2015

KEYWORDS

Aero-engine casings;
Bull-nose end mill;
Chatter;
Four-axis milling;
Stability lobe diagram

Abstract An analytical model for chatter stability prediction in bull-nose end milling of aero-engine casings is presented in this paper. And the mechanics and dynamics variations due to the complex cutter and workpiece geometry are considered by analyzing the effects of the lead angle on the milling process. Firstly, the tool-workpiece engagement region is obtained by using a previously developed method and divided into several disk elements along the tool-axis direction. Secondly, a 3D dynamic model for stability limit calculation is developed and simplified into a 1D model in normal direction considering only the dominant mode of the workpiece. Then the cutting force coefficients, the start and exit angles corresponding to each disk element are determined. And the total stability lobe diagram is calculated using an iterative algorithm. Finally, several experimental tests are carried out to validate the feasibility and effectiveness of the proposed prediction approach.

© 2015 The Authors. Production and hosting by Elsevier Ltd. on behalf of CSAA & BUAA. This is an open access article under the CC BY-NC-ND license (http://creativecommons.org/licenses/by-nc-nd/4.0/).

1. Introduction

Thin-walled parts have been widely used in the aerospace industry, such as aero-engine casings, blades and impellers. They can significantly help to improve the working performance of aircraft. However, due to the complex structures and weak rigidity of their own, they also bring many machining difficulties and challenges. Chatter is one of the main machining problems, which leads to poor surface finish and low production efficiency.[1–16] In order to avoid chatter, the milling process must be conducted in a stable state. Thus, the machining stability prediction becomes very important in achieving good machining quality and high productivity. Many studies have been focused on this issue.

Tobias and Fishwick[1], as well as Tlusty and Polacek[2] developed the stability lobe theory in orthogonal cutting process, which makes it possible to predict the chatter phenomena of milling process. Altintas and Budak[3] presented an analytical method to generate stability lobe diagram directly in the frequency domain. They considered the average term in the Fourier series expansions as the approximation of time-varying directional coefficients and used an eigenvalue solution to solve the critical depth of cut. However, the single-frequency method cannot predict the additional stability region and the

* Corresponding author. Tel.: +86 29 88493009.
E-mail address: dhzhang@nwpu.edu.cn (D. Zhang).

Peer review under responsibility of Editorial Committee of CJA.

Production and hosting by Elsevier

http://dx.doi.org/10.1016/j.cja.2015.06.001
1000-9361 © 2015 The Authors. Production and hosting by Elsevier Ltd. on behalf of CSAA & BUAA.
This is an open access article under the CC BY-NC-ND license (http://creativecommons.org/licenses/by-nc-nd/4.0/).

doubling bifurcations at small radial immersions.[4–7] To overcome this problem, Budak and Altintas[4,5] developed a multi-frequency solution of chatter stability, which includes the higher order terms of the Fourier series expansions. And Merdol and Altintas[6], Gradišeka et al.[7] extended the multi-frequency approach and the semi-discretization method to the milling cases of low radial immersion.

The dynamics of flat end milling are considered in the transversal directions of the cutter. However, for ball and bull-nose end milling, the dynamics must be considered in all the three directions.[8–16] Altintas[8] extended the two dimensional chatter stability theory to a three-dimensional chatter problem by adding the dynamics in the tool-axis direction. Based on this work, Seguy et al.[9], Campa et al.[10,11] and Adetoro et al.[12,13] calculated the stability lobe diagrams in bull-nose end milling of thin floors and thin walls by considering the nonlinearities of the axial immersion angle and the cutting force coefficients. For multi-axis milling, the effects of tool positions on the process geometry, mechanics and dynamics cannot be ignored. Shamoto and Akazawa[14], Budak and Ozturk[15,16] studied the influences of lead and tilt angles on the engagement region and predicted the chatter stability of five-axis ball end milling.

Aeroengine casings are typical thin-walled parts with ring-shaped and closed geometry structures and also present machining problems due to chatter. However, unlike the milling of thin plates, the dynamics in the milling of aero-engine casings is more complex owing to the symmetry of the structure and the support of the fixture.[17,18] The cutting deformation and vibration occur mainly in radial direction of the part and have a certain symmetry in circumferential direction of the part. The thinner the wall thickness is, the worse the cutting deformation and vibration become. And the dynamics of the process system such as the natural frequency and the stiffness will change significantly in the material removal process, even a small part of the undesired material is removed. Normally, the aero-engine casings are fixed by the axial pressing and radial supporting forms. And the dynamics of the part will be significantly different with different pressing forces or different supporting positions. All the above factors will make the milling process exhibit the nonlinear and strong time-varying characteristics, thus inducing drastic cutting chatter. Therefore, chatter prediction and suppression in the milling of aero-engine casings become more difficult.

In this paper, a calculation method of stability lobe diagrams in four-axis bull-nose end milling of aero-engine casings is presented. Firstly, the tool-workpiece engagement region is determined by considering the influences of lead angle. And based on the engagement region, the start and exit angles of each disk element, the directional coefficients can be obtained. Secondly, the chatter stability model is developed and simplified to 1D model by considering only the normal direction dynamics. And the total stability lobe diagram is obtained by using an iterative algorithm. Lastly, several milling tests verifies the feasibility and effectiveness of the chatter stability prediction method.

2. Chatter stability model

The chatter stability model used in this paper is the 3D model proposed by Altintas.[8] And the effects of lead angle on the engagement region, thus, on the directional coefficients are also discussed. The helix angle and the process damping are not taken into account in this chatter theory.

2.1. Calculation of tool-workpiece engagement region

In order to calculate the tool-workpiece engagement region, three coordinate systems are defined in four-axis milling process, as shown in Fig. 1. The first one is a fixed coordinate system, MCS, formed by the X, Y and Z axes of the machine tool. The second one is the process coordinate system, FCN, consisting of feed F, cross-feed C and surface normal N axes. x, y, z are the tool-axis coordinate in the TCS. The last one

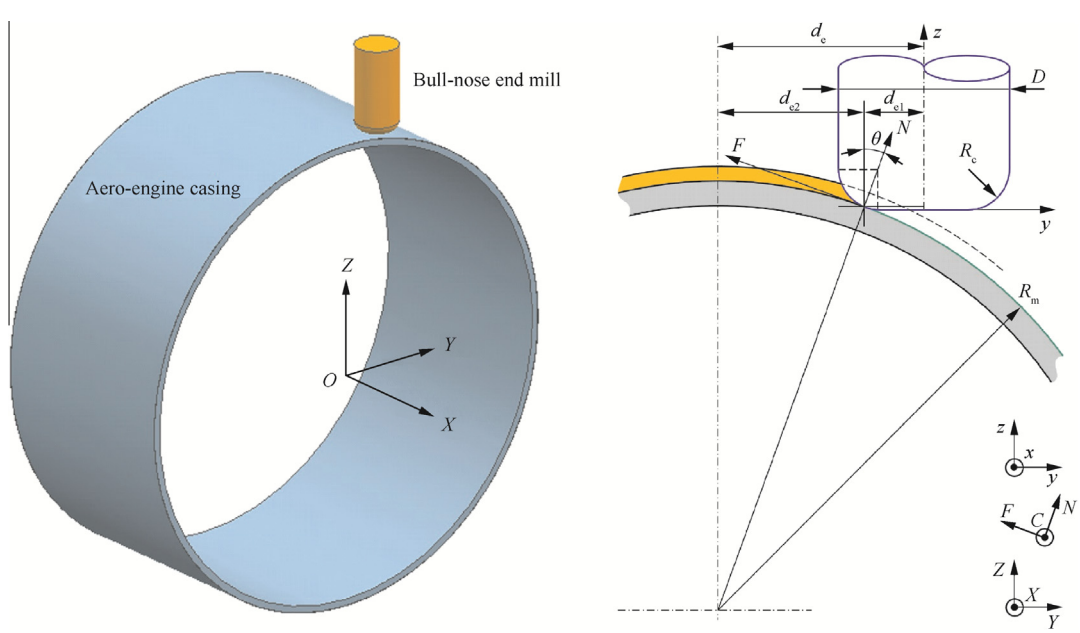

Fig. 1 Coordinate systems and lead angle.

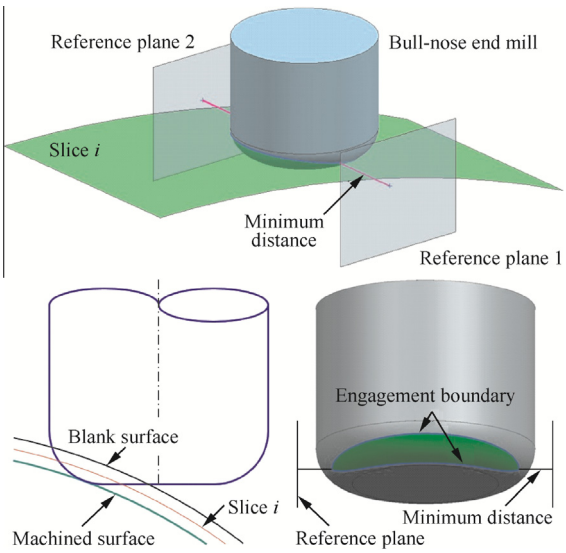

Fig. 2 Calculation of engagement region.

is the tool coordinate system, TCS, which is the rotated form of the FCN. In FCN, the tool-axis direction is defined by a lead angle θ, which can be determined as

$$\theta = \arcsin \frac{d_{e1} - \left(\frac{D}{2} - R_c\right)}{R_c} \tag{1}$$

with

$$\theta = \arcsin \frac{d_{e2}}{R_m} \tag{2}$$

$$d_e = d_{e1} + d_{e2} \tag{3}$$

where D is the cutter diameter, R_c the cutter corner radius, R_m the machined surface radius, d_e the eccentric distance, d_{e1} the first part of the eccentric distance and d_{e2} the second part of the eccentric distance.

The engagement region is located between the toroidal surface rotated by cutter edges and the workpiece solid, as shown in Fig. 2. In this paper, the previously developed method[19] is extended to calculate the tool-workpiece engagement region. The algorithm is as follows. Firstly, several slices are inserted between the machined and blank surfaces to get the intersection curves between the slices and the toroidal surface. Secondly, by determining the minimum distance from the intersection curves to the reference planes, the reference points can be obtained. Then, the engagement boundary can be fixed with a spline curve fitted by the reference points and an intersection curve between the blank surface and the toroidal surface. This method can be used in three different cutting cases: first cut, following cut and slotting cut.

2.2. Calculation of dynamic cutting forces

During the milling process, the cutting forces excite the workpiece and then cause dynamic displacements in all three directions, as shown in Fig. 3. k_X, k_Y and k_Z are the X, Y and Z axial stiffness in the MCS, respectively. c_X, c_Y and c_Z are the X, Y and Z axial damping in the MCS, respectively. The dynamic displacements lead to a modulated chip thickness, which consists of two components: the static and dynamic chip thickness. The static chip thickness can be removed since it does not contribute to the chatter stability. The dynamic chip thickness between the present edge and the previous edge can be calculated as

$$h_j(\phi_j, \gamma) = (\Delta r \sin\gamma - \Delta z \cos\gamma) g(\phi_j) \tag{4}$$

with

$$\Delta r = \Delta x \sin\phi_j + \Delta y \cos\phi_j \tag{5}$$

$$\begin{cases} \Delta x = x(t) - x(t-T) \\ \Delta y = y(t) - y(t-T) \\ \Delta z = z(t) - z(t-T) \end{cases} \tag{6}$$

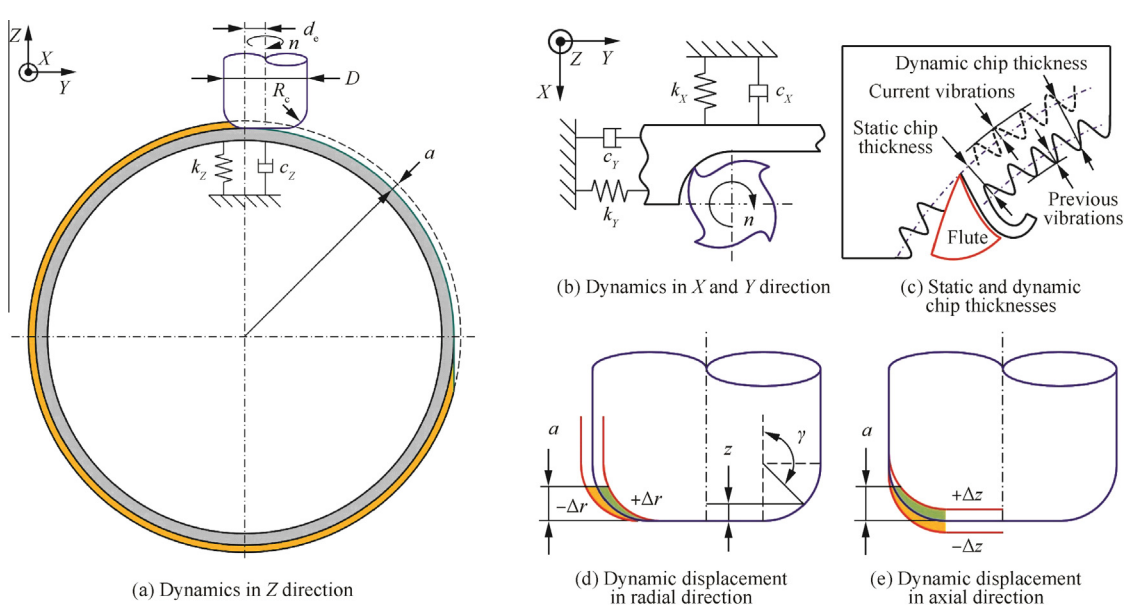

Fig. 3 Dynamic milling model for bull-nose end milling of aero-engine casings.

$$g(\phi_j) = \begin{cases} 0 & \text{for otherwise} \\ 1 & \text{for } \phi_{st} < \phi_j < \phi_{ex} \end{cases} \tag{7}$$

where ϕ_j is the instantaneous angular immersion of tooth j, γ the axial immersion angle and Δr the radial dynamic displacement. Δx, Δy and Δz are the x, y and z axial dynamic displacements in the TCS, respectively. $x(t)$, $y(t)$, $z(t)$ and $x(t-T)$, $y(t-T)$, $z(t-T)$ represent the relative dynamic displacements between the workpiece and cutter at the present time t and previous tooth periods $t-T$, respectively. T the tooth passing period. $g(\phi_j)$ is a unit step function. ϕ_{st} and ϕ_{ex} are the start and exit angles, respectively.

For a bull-nose end mill, the axial immersion angle γ is variable along the tool-axis direction. And it can be expressed as

$$\gamma = \begin{cases} \pi - \arccos\frac{R_c - z}{R_c} & \text{for } z \leqslant R_c \\ \dfrac{\pi}{2} & \text{for } z > R_c \end{cases} \tag{8}$$

The cutting forces are normally separated into edge and cutting components in the linear force model. The edge forces caused by the plowing between flank face of the cutter and the finished surface can be expressed as the product of the edge force coefficients and the length of the elemental edge. While the cutting forces caused by the shearing of material at the rake face can be expressed as the product of the cutting force coefficients, the uncut chip thickness and the chip width. The edge forces do not take into account the chatter stability model, as they are not related to the chip thickness, in other words, they do not contribute to the regenerative chatter. The dynamic cutting forces on tooth j in the tangential, radial and axial directions can be defined as

$$\begin{cases} F_{t,j}(\phi_j,\gamma) = K_t a h_j(\phi_j,\gamma) \\ F_{r,j}(\phi_j,\gamma) = K_r a h_j(\phi_j,\gamma) \\ F_{a,j}(\phi_j,\gamma) = K_a a h_j(\phi_j,\gamma) \end{cases} \tag{9}$$

where K_t, K_r and K_a are the tangential, radial and axial cutting force coefficients, respectively. a is the axial depth of cut.

Then those forces can be mapped into Cartesian coordinate system as follows:

$$\begin{bmatrix} F_{x,j}(\phi_j,\gamma) \\ F_{y,j}(\phi_j,\gamma) \\ F_{z,j}(\phi_j,\gamma) \end{bmatrix} = \boldsymbol{M} \begin{bmatrix} F_{t,j}(\phi_j,\gamma) \\ F_{r,j}(\phi_j,\gamma) \\ F_{a,j}(\phi_j,\gamma) \end{bmatrix} \tag{10}$$

with

$$\boldsymbol{M} = \begin{bmatrix} -\cos\phi_j & -\sin\gamma\sin\phi_j & \cos\gamma\sin\phi_j \\ \sin\phi_j & -\sin\gamma\cos\phi_j & \cos\gamma\cos\phi_j \\ 0 & -\cos\gamma & -\sin\gamma \end{bmatrix} \tag{11}$$

Substituting Eq. (9) into Eq. (10) and summing the cutting forces contributed by all cutting edges, the total dynamic milling forces can be obtained as:

$$\begin{bmatrix} F_x(t) \\ F_y(t) \\ F_z(t) \end{bmatrix} = a K_t \boldsymbol{A}_0 \begin{bmatrix} \Delta x \\ \Delta y \\ \Delta z \end{bmatrix} \tag{12}$$

where $F_x(t)$, $F_y(t)$ and $F_z(t)$ are the cutting forces along the x-, y- and z-axis directions in time domain, respectively. $\boldsymbol{A}_0$ is the matrix of directional coefficients.[8]

Using the mono-frequency solution, Eq. (12) can be reduced to Eq. (13):

$$\begin{bmatrix} F_x(t) \\ F_y(t) \\ F_z(t) \end{bmatrix} = \frac{N_f}{4\pi} a K_t \boldsymbol{A}_1 \begin{bmatrix} \Delta x \\ \Delta y \\ \Delta z \end{bmatrix} \tag{13}$$

where N_f is the flute number and $\boldsymbol{A}_1$ the directional factor matrix.

2.3. Calculation of stability limit

Using the transfer function at the cutter-workpiece contact area, the dynamic displacements can be described in frequency domain:

$$\begin{bmatrix} \Delta x(i\omega_c) \\ \Delta y(i\omega_c) \\ \Delta z(i\omega_c) \end{bmatrix} = \left(1 - e^{-i\omega_c T}\right)\boldsymbol{G} \begin{bmatrix} F_x(i\omega_c) \\ F_y(i\omega_c) \\ F_z(i\omega_c) \end{bmatrix} e^{i\omega_c T} \tag{14}$$

where ω_c is the chatter frequency. $\boldsymbol{G} = \boldsymbol{G}_c + \boldsymbol{G}_w$ is the sum of the transfer function matrixes of the cutter and the workpiece.

Therefore, Eq. (13) can be expressed as

$$\begin{bmatrix} F_x(i\omega_c) \\ F_y(i\omega_c) \\ F_z(i\omega_c) \end{bmatrix} = \frac{N_f}{4\pi} a K_t (1 - e^{-i\omega_c T}) \boldsymbol{A}_1 \boldsymbol{G} \begin{bmatrix} F_x(i\omega_c) \\ F_y(i\omega_c) \\ F_z(i\omega_c) \end{bmatrix} \tag{15}$$

Then Eq. (15) becomes an eigenvalue problem, where Eq. (16) defines the stability and Eq. (17) defines the eigenvalue λ .

$$\det\{\boldsymbol{I} + \lambda \boldsymbol{A}_1 \boldsymbol{G}\} = 0 \tag{16}$$

$$\lambda = -\frac{N_f}{4\pi} a K_t \left(1 - e^{-i\omega_c T}\right) \tag{17}$$

The critical axial depth of cut a_{lim} and the corresponding spindle speeds n for each lobe k are obtained as

$$a_{lim} = -\frac{2\pi \mathrm{Re}(\lambda)}{N_f K_t}\left[1 + \left(\frac{\mathrm{Im}(\lambda)}{\mathrm{Re}(\lambda)}\right)^2\right] \tag{18}$$

$$n = \frac{60\omega_c}{N_f\left[(2k+1)\pi - 2\arctan\left(\frac{\mathrm{Im}(\lambda)}{\mathrm{Re}(\lambda)}\right)\right]} \tag{19}$$

2.4. Simplified 1D model for four-axis milling

During the bull-nose end milling of aero-engine casings, a small lead angle is required to keep the bottom cutting edges from cutting materials, thus achieving a better surface finish. The smaller the lead angle is, the bigger the cutting width becomes. In addition, a small lead angle can meet the needs of tool-axis directions because the outer surfaces of aero-engine casings have relatively open spaces.

For the milling of aero-engine casings, the tool is rigid compared to the workpiece. In other words, the workpiece is considered to be flexible. And the displacement of the workpiece occurs only along the normal direction. When the lead angle is equal to zero, the surface normal direction coincides with the tool-axis direction. However, when the lead angle is equal to a small value, the dynamic displacement in surface normal direction can be approximated by the dynamic displacement in z direction. And the dynamic displacements in x and y directions can be ignored because they are minor compared to the dominant mode. Hence, the chatter stability model presented

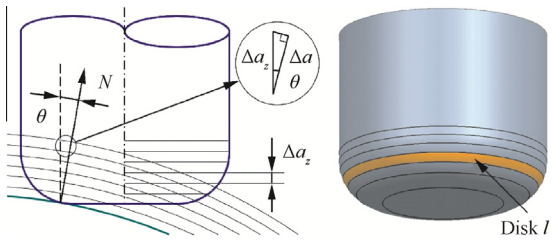

Fig. 4 Mechanics and dynamics of disk l.

here can be reduced to a 1D model in the normal direction. The stability problem in Eq. (15) can be simplified into

$$F_z(\mathrm{i}\omega_c) = \frac{N_f}{4\pi} a K_t \left(1 - \mathrm{e}^{-\mathrm{i}\omega_c T}\right) \alpha_{zz} G_z(\mathrm{i}\omega_c) F_z(\mathrm{i}\omega_c)$$
$$= \frac{N_f}{2\pi} a K_t \alpha_{zz} \mathrm{Re}[G_z(\mathrm{i}\omega_c)] F_z(\mathrm{i}\omega_c) \tag{20}$$

with

$$\alpha_{zz} = \phi[-K_r(cos2\gamma + 1) + K_a \sin 2\gamma]_{\phi_{st}}^{\phi_{ex}} \tag{21}$$

$$\mathrm{Re}[G_z(\mathrm{i}\omega_c)] = \frac{1 - d_z^2}{k_z\left[\left(1 - d_z^2\right)^2 + (2\xi_z d_z)^2\right]} \tag{22}$$

where $d_z = \omega_c/\omega_n$, ω_n is the natural frequency of the mode. k_z the stiffness and ξ_z the damping ratio.

When the lead angle θ is equal to 0 degree, the cutting depth a is defined along both the tool-axis and surface normal directions. However, in four-axis milling process, the axial depth of cut a_z varies as the lead angle θ changes, as shown in Fig. 4. And it can be determined as

$$a_z = \frac{a}{\cos\theta} \tag{23}$$

Then the stability problem in four-axis milling process can be obtained:

$$F_z(\mathrm{i}\omega_c) = \frac{N_f}{2\pi\cos\theta} a K_t \alpha_{zz} \mathrm{Re}[G_z(\mathrm{i}\omega_c)] F_z(\mathrm{i}\omega_c) \tag{24}$$

Because of the complex cutter and workpiece geometry, the cutting force coefficients, the start and exit angles are not constant along the tool-axis direction. Then a disk-based method developed by Budak and Ozturk[15,16] is extended to calculate the stability limit in four-axis milling of aero-engine casings.

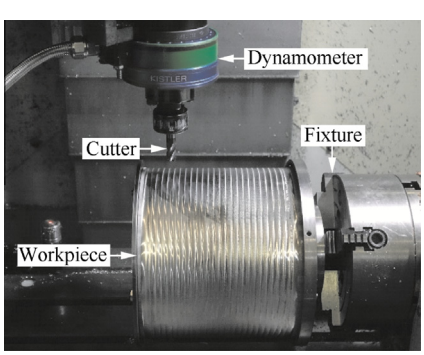

Fig. 5 Experimental setup of aero-engine casing milling.

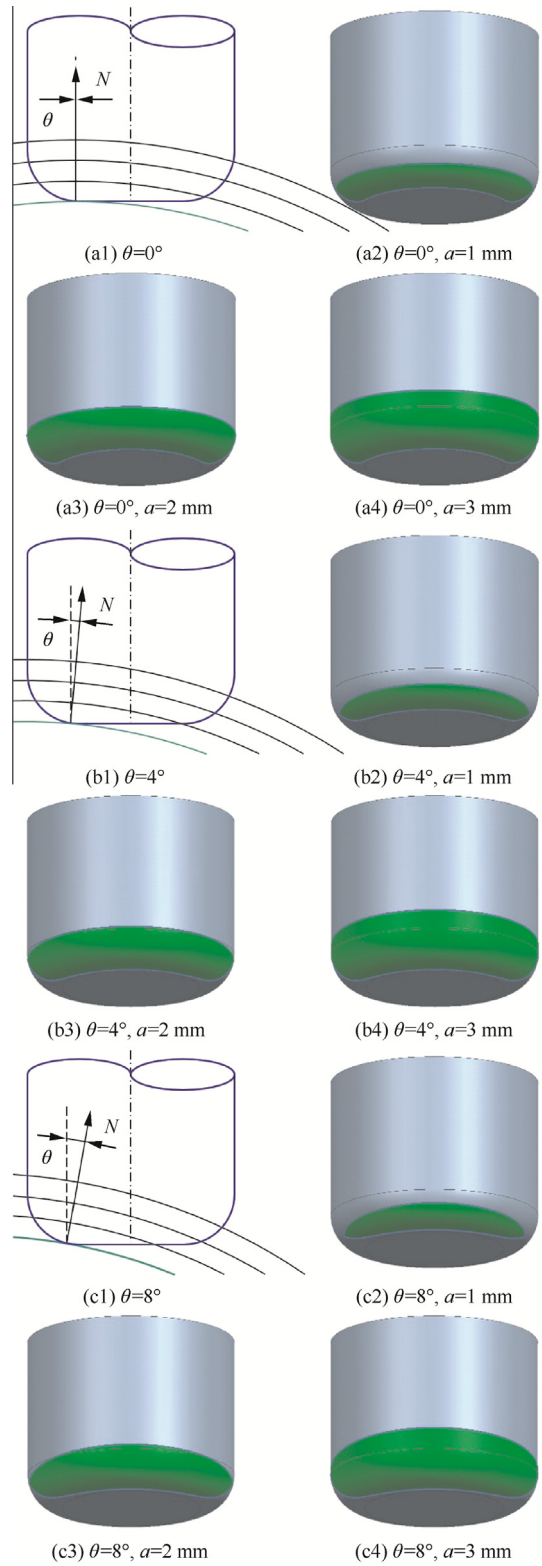

Fig. 6 Tool-workpiece engagement regions with three different lead angles.

The bull-nose end mill is divided into several disk elements along the tool-axis direction. And each disk element has a height of Δa. For the disk l, the stability problem in Eq. (24) can be expressed as

$$F_z^l(\mathrm{i}\omega_c) = \frac{N_f}{2\pi cos\theta}\Delta a K_t^l \alpha_{zz}^l \mathrm{Re}[G_z(\mathrm{i}\omega_c)]F_z^l(\mathrm{i}\omega_c) \tag{25}$$

In order to obtain the total stability limit of the process system, the dynamics of all the disk elements have to be summed up:

$$F_z(\mathrm{i}\omega_c) = \frac{N_f}{2\pi cos\theta}\Delta a\left(\sum_{l=1}^{m} K_t^l \alpha_{zz}^l\right)\mathrm{Re}[G_z(\mathrm{i}\omega_c)]F_z(\mathrm{i}\omega_c) \tag{26}$$

where m is the total number of disk elements.

Then the stability limit corresponding to Δa is obtained:

$$\Delta a_{\lim} = \frac{2\pi cos\theta}{N_f\left(\sum_{l=1}^{m} K_t^l \alpha_{zz}^l\right)\mathrm{Re}[G_z(\mathrm{i}\omega_c)]} \tag{27}$$

And the spindle speed is expressed as follows:

$$n = \frac{30\omega_c}{N_f\left[(k+1)\pi - \arctan\left(\frac{d_z^2-1}{2\xi_z d_z}\right)\right]} \tag{28}$$

Because there are m disks in the calculation, the total stability limit for a given chatter frequency ω_c is calculated in the following form:

$$a_{\lim} = m\Delta a_{\lim} \tag{29}$$

In the solution of the stability limits, the following procedure is used. Firstly, the cutting depth a begins from an initial value Δa and increases with a step size Δa.

And for each cutting depth, the tool-workpiece engagement region is determined. Secondly, the total stability lobe diagram can be obtained by sweptwing the chatter frequency ω_c around a predetermined chatter frequency range. The calculation process will not stop until all the determined stability limits $a_{\lim}$ in the stability lobe diagram are less than the cutting depth a.

3. Experimental results and discussion

To validate the proposed method, several milling tests were carried out on a high-speed milling center, as shown in Fig. 5. Cemented carbide and 304 stainless steel were used as the cutter and the workpiece materials, respectively. The tool is a bull-nose end mill with 4 flute, 12 mm diameter, 2 mm corner radius and 30° helix angle. The workpiece is a cylindrical pipe with 211 mm inner diameter and 217 mm outer diameter. The milling tests are a series of slotting, where the feed rate is 320 mm/min, the axial depth of cut is 0.5 mm and 1.0 mm and the radial depth of cut is 12 mm. In order to ensure the consistency of dynamics along the circumferential direction, the aeroengine casing was fixed by axial pressing without other supporting forms.

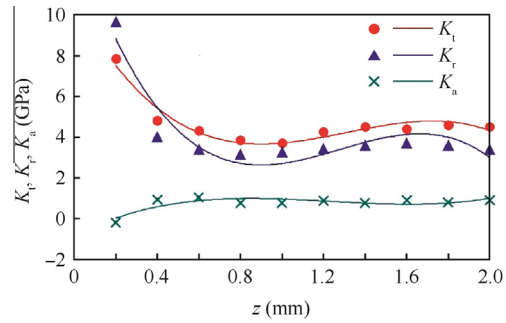

Fig. 7 Cutting force coefficients.

Table 2 Modal parameters of workpiece.

ω_n (Hz)	ξ_z	k_z(N/m)		
		$\theta = 0°$	$\theta = 4°$	$\theta = 8°$
794.384	0.036	4.247×10^7	4.258×10^7	4.289×10^7

Based on the previously developed engagement model, several tool-workpiece engagement regions with three different lead angles are calculated as shown in Fig. 6. For each engagement region, several disk elements are obtained in tool-axis direction. And start and exit angles for each disk are determined and given in Table 1.

The cutting force coefficients are calculated as functions of the tool-axis coordinate using the approach developed by Gao et al.[20] as shown in Fig. 7. With elevation z as the independent variable, the cutting force coefficients corresponding to each disk can be obtained.

The modal parameters of the aeroengine casing measured by using impact tests and finite element simulations are listed in Table 2. The locations for the milling and impact tests are consistent.

Table 1 Start and exit angles for each disk with three different lead angles.

Lead angle	Item	Disk										
		1	2	3	4	5	6	7	8	9	10	11
0°	ϕ_{st} (rad)	0.0995	0.0555	0.0410	0.0319	0.0249	0.0192	0.0142	0.0097	0.0057	0.0018	0.0000
	ϕ_{ex} (rad)	3.0421	3.0861	3.1006	3.1097	3.1167	3.1224	3.1274	3.1319	3.1359	3.1398	3.1416
	z (mm)	0.1000	0.3000	0.5000	0.7000	0.9000	1.1000	1.3000	1.5000	1.7000	1.9000	2.1000
4°	ϕ_{st} (rad)	0.2887	0.1611	0.1154	0.0879	0.0680	0.0523	0.0391	0.0272	0.0159	0.0051	0.0000
	ϕ_{ex} (rad)	2.8529	2.9805	3.0262	3.0537	3.0736	3.0893	3.1025	3.1144	3.1257	3.1365	3.1416
	z (mm)	0.1049	0.3049	0.5049	0.7049	0.9049	1.1049	1.3049	1.5049	1.7049	1.9049	2.1049
8°	ϕ_{st} (rad)	0.4638	0.2642	0.1886	0.1440	0.1114	0.0854	0.0636	0.0438	0.0252	0.0072	0.0000
	ϕ_{ex} (rad)	2.6778	2.8774	2.9530	2.9976	3.0302	3.0562	3.0780	3.0978	3.1164	3.1344	3.1416
	z (mm)	0.1195	0.3195	0.5195	0.7195	0.9195	1.1195	1.3195	1.5195	1.7195	1.9195	2.1195

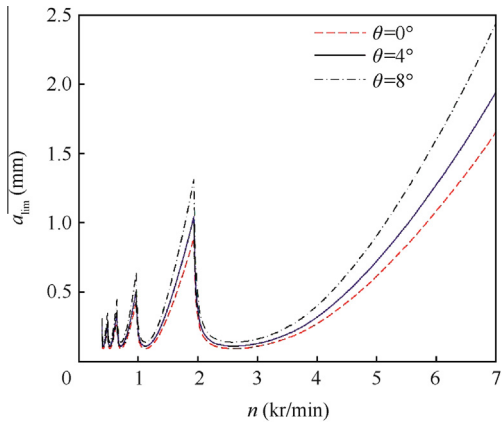

Fig. 8 Stability lobe diagrams at different lead angles.

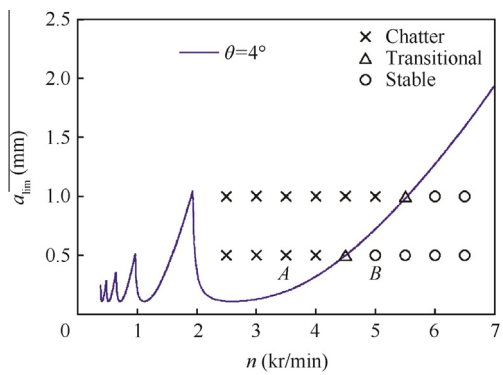

Fig. 9 Stability lobe diagram for 4° lead angle.

Then the stability lobe diagrams for four-axis milling of aeroengine casing with different lead angles can be calculated by the presented approach as shown in Fig. 8. It can be found that the chatter stability boundary grows in the vertical direction which does not move in the horizontal direction with the increase of lead angle. For a fixed milling system, the larger the lead angle, the greater the minimum stability limit. This is because the tool-workpiece engagement region will become smaller as the lead angle increases. And the interaction between the cutter and the workpiece will become weak.

In the stability lobe diagram of 4° lead angle, there are three different cutting status: chatter, transitional and stable, as shown in Fig. 9. The transitional cutting status means that the predicted chatter frequency can be seen very slightly in the spectrum of the measured force. This status often appears near the chatter stability boundary in the stability lobe diagram. And the unstable and stable zones can be seen above and below the chatter stability boundary, respectively.

The normal cutting force data and the corresponding spectra at two points (points *A* and *B* in Fig. 9) are presented in Fig. 10. The cutting status at point *A* with a spindle speed of 3500 r/min and cutting depth of 0.5 mm is unstable with a chatter frequency of 594.0 Hz. It can be seen that the amplitude at the chatter frequency is higher than the amplitude at the tooth passing frequency, which demonstrates that the milling process is unstable. While the cutting status at point *B* with a spindle speed of 5000 r/min and cutting depth of 0.5 mm is stable. For point *B*, the maximum amplitude occurs at a tooth passing frequency of 333.3 Hz in the cutting force spectrum, whereas the amplitude at the natural frequency of the workpiece is very small. The surface finishes for the points *A* and *B* are also shown in Fig. 10. And the cutting marks validate the accuracy of the proposed prediction approach.

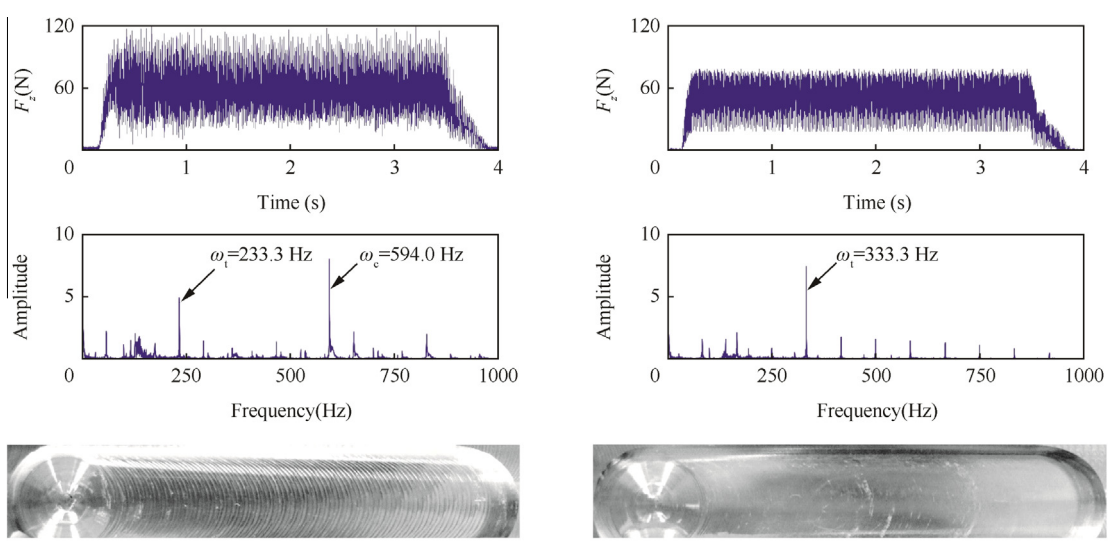

(a) Point *A* (b) Point *B*

Fig. 10 Cutting forces and machined surfaces for points *A* and *B*.

4. Conclusions

(1) A 3D chatter stability model for bull-nose end milling of aeroengine casings is developed in this paper. And the 3D model can be simplified to a 1D model in surface normal direction considering only the dominant mode of the workpiece.
(2) The model is extended to four-axis machining by adding the effects of the lead angle in the milling process. The tool-workpiece engagement region is determined by using a slice-based method and divided along the tool-axis direction into several disks. And the total stability lobe diagram for the process system is obtained by an iterative algorithm.
(3) The model and approach are validated by analyzing experimental results and a good agreement has been achieved.
(4) The proposed method can be used to predict chatter stability in four-axis milling of aeroengine casings, where a small lead angle should be selected. While for the case of large lead angle or five-axis milling, the 3D model that will be developed in the future must be used because the dynamic displacements in all three directions play important roles in the regenerative chatter.

Acknowledgements

This work was supported by the National Basic Research Program of China (No. 2013CB035802) and the 111 Project of China (No. B13044).

References

1. Tobias SA, Fishwick W. A theory of self regenerative chatter. *The Engineer* 1958;**205**:199–203.
2. Tlusty J, Polacek M. The stability of machine tools against self-excited vibrations in machining. *Proceedings of the international research in production engineering;* 1963 September 9–12; Pittsburgh, PA, USA. New York: ASME; 1963. p. 465–74.
3. Altintas Y, Budak E. Analytical prediction of stability lobes in milling. *CIRP Ann Manuf Technol* 1995;**44**(1):357–62.
4. Budak E, Altintas Y. Analytical prediction of chatter stability in milling – part I: general formulation. *J Dyn Sys Meas Control* 1998;**120**(1):22–30.
5. Budak E, Altintas Y. Analytical prediction of chatter stability in milling – part II: application of the general formation to common milling systems. *J Dyn Sys Meas Control* 1998;**120**(1):31–6.
6. Merdol SD, Altintas Y. Multi frequency solution of chatter stability for low immersion milling. *J Manuf Sci Eng* 2004;**126**(3):459–66.
7. Gradišeka J, Govekara E, Grabeca I, Kalveramb M, Weinertb K, Inspergerc T, et al. On stability prediction for low radial immersion milling. *Mach Sci Technol* 2005;**9**(1):117–30.
8. Altintas Y. Analytical prediction of three dimensional chatter stability in milling. *JSME Int J Ser C* 2001;**44**(3):717–23.
9. Seguy S, Campa FJ, López de Lacalle LN, Arnaud L, Dessein G, Aramendi G. Toolpath dependent stability lobes for the milling of thin-walled parts. *Int J Mach Mach Mater* 2008;**4**(4):377–92.
10. Campa FJ, López de Lacalle LN, Lamikiz A, Sánchez JA. Selection of cutting conditions for a stable milling of flexible parts with bull-nose end mills. *J Mater Process Technol* 2007;**191**(1-):279–82.
11. Campa FJ, López de Lacalle LN, Celaya A. Chatter avoidance in the milling of thin floors with bull-nose end mills: Model and stability diagrams. *Int J Mach Tools Manuf* 2011;**51**(1):43–53.
12. Adetoro OB, Sim WM, Wen PH. An improved prediction of stability lobes using nonlinear thin wall dynamics. *J Mater Process Tech* 2010;**210**(6–7):969–79.
13. Adetoro OB, Sim WM, Wen PH. Stability lobes prediction for corner radius end mill using nonlinear cutting force coefficients. *Mach Sci Technol* 2012;**16**(1):111–30.
14. Shamoto E, Akazawa K. Analytical prediction of chatter stability in ball end milling with tool inclination. *CIRP Ann Manuf Technol* 2009;**58**(1):351–4.
15. Budak E, Ozturk E, Tunc LT. Modeling and simulation of 5-axis milling processes. *CIRP Ann Manuf Technol* 2009;**58**(1):347–50.
16. Ozturk E, Budak E. Dynamics and stability of five-axis ball-end milling. *J Manuf Sci Eng* 2010;**132**(2):021003-1–13.
17. Chen D, Lin B, Han ZL, Zhang YB. Study on the optimization of cutting parameters in turning thin-walled circular cylindrical shell based upon cutting stability. *Int J Adv Manuf Technol* 2013;**69**(1–4):891–9.
18. Kolluru K, Axinte D. Coupled interaction of dynamic responses of tool and workpiece in thin wall milling. *J Mater Process Technol* 2013;**213**(9):1565–74.
19. Wu BH, Gao G, Luo M, Xie GN. Prediction and experimental validation of cutting force for bull-nose end mills with lead angle. *Adv Mech Eng* 2014;**2014**:650215-1–15.
20. Gao G, Wu BH, Zhang DH, Luo M. Mechanistic identification of cutting force coefficients in bull-nose milling process. *Chin J Aeronaut* 2013;**26**(3):823–30.

Zhou Xu received his B.S. and M.S. degrees from Northwestern Polytechnical University in 2009 and 2012, respectively, and is now a Ph. D. candidate there. His main research interests are multi-axis machining and high-speed machining.

Zhang Dinghua received his B.S., M.S. and Ph.D. degrees from Northwestern Polytechnical University in 1981, 1984 and 1989, respectively, and is now a professor there. His main research interests are multi-axis machining, high-speed machining, machining surface integrity and industrial CT technology.